

Characterizing the intracrustal low velocity zone beneath northwest India–Asia collision zone

Devajit Hazarika, Koushik Sen and Naresh Kumar

Wadia Institute of Himalayan Geology, Dehradun 248 001, India. E-mail: devajit_01@yahoo.com

Accepted 2014 August 22. Received 2014 August 19; in original form 2013 December 20

SUMMARY

Teleseismic data recorded at 13 broad-band seismological stations across northwest part of the Tethyan Himalaya and eastern Ladakh are analysed to determine the seismic characteristics of the crust and upper mantle beneath the northwest India–Asia collision zone. The receiver functions computed from teleseismic *P*-waveform for a wide range of backazimuth show strong azimuthal variation in the Indus suture zone (ISZ), the zone which marks the collision and subsequent subduction of both the Tethyan oceanic plate and Indian continental plate beneath Eurasia. The teleseismic waves piercing the ISZ do not show clear *P*-to-*S* (*Ps*) converted phase at the depth of Moho. In contrast, the waves piercing the Karakoram zone, Ladakh batholith and the Tethyan Himalayan region south of the ISZ clearly show the Moho converted *Ps* phase and corresponding inverted models reveal variation of crustal thickness from ~60 km beneath the Tethyan Himalaya to ~80 km beneath the Karakoram fault zone. A prominent intracrustal low velocity zone (IC-LVZ) is detected in the shear wave velocity models within the depth range ~15–40 km. The IC-LVZ identified at the stations both north and south of the ISZ can be interpreted as due to presence of fluid/partial melt. Our study provides compelling evidence that the mid-crustal low velocity zone does extend across the suture zone, in to the Tethyan Himalaya. The contact between this serpentinized ultramafic rocks and the eclogitized Indian continental crust in the suture zone is identified at ~47–50 km depth.

Key words: Ultra-high pressure metamorphism; Mantle processes; Crustal structure.

1 INTRODUCTION

The northwest Himalaya and Ladakh–Karakoram region outline the western extremity of the Himalayan–Tibetan orogenic system which provides unique opportunity to study the interaction of the Indian and Eurasian plates. The Indus suture zone (ISZ) is a major tectonic unit well exposed in this part of orogenic system which separates Eurasian continental plate lying to its north from the Indian Plate to the south (Fig. 1). This orogenic system has been evolved as a result of subduction of the Tethyan oceanic crust until collision, followed by underthrusting of the Indian continental margin beneath the Eurasian Plate (Honegger *et al.* 1982; Searle *et al.* 1987; Guillot *et al.* 2000). The eastern part of Ladakh region is considered as a subduction complex that records the subduction of the Tethyan oceanic lithosphere and finally the collision and subduction of the Indian continental margin beneath Eurasia at ~55 Ma (Guillot *et al.* 2003). The tectonic setting of this region is distinctive where an ophiolitic suite, the Nidar Ophiolitic Complex (NOC), is sandwiched between Ultra-High Pressure (UHP) rocks of Tso Morari Crystallines (TMC) of Indian continental affinity and the Ladakh magmatic arc.

The geology of the region indicates deep subduction process of the leading edge of the Indian continental margin beneath the Eurasian Plate as evidenced by coesite-bearing UHP eclogites

exposed in the TMC (Mukherjee & Sachan 2004; Leech *et al.* 2005). The geophysical studies also support the underthrusting of Indian continental crust beneath the Eurasian Plate (Rai *et al.* 2006; Oreshin *et al.* 2008, 2011; Chamoli *et al.* 2011). The receiver function (RF) studies reveal a continuous dipping of Moho starting from ~40 km at frontal part of the Himalaya to ~75 km in the Ladakh–Karakoram zone (Rai *et al.* 2006; Oreshin *et al.* 2008). These RF studies primarily focused on the regional scale variation of first order discontinuities (e.g. Moho), with less emphasis on intracrustal features. The magnetotelluric (MT) investigations carried out across the TMC and ISZ identified a low resistivity zone in the crust which was interpreted as due to the presence of partial melt/serpentinites (Gokarn *et al.* 2002; Arora *et al.* 2007). A subvertical and northeasterly dipping nature of the ISZ was suggested by Arora *et al.* (2007). Characteristic of seismic waves detect fluid reach zones as a low shear wave velocity zone beneath Ladakh (Caldwell *et al.* 2009; Rai *et al.* 2009; Hazarika *et al.* 2013). The Rayleigh wave dispersion study by Caldwell *et al.* (2009) observed a pronounced intracrustal low velocity zone (IC-LVZ) centred at ~30 km depth beneath Ladakh. This study suggested presence of fluid or partial melt in the mid-crustal depth. Similar inference is also evidenced by high Lg wave attenuation and high average crustal Poisson's ratio existing beneath the region (Rai *et al.* 2009; Hazarika *et al.* 2013).

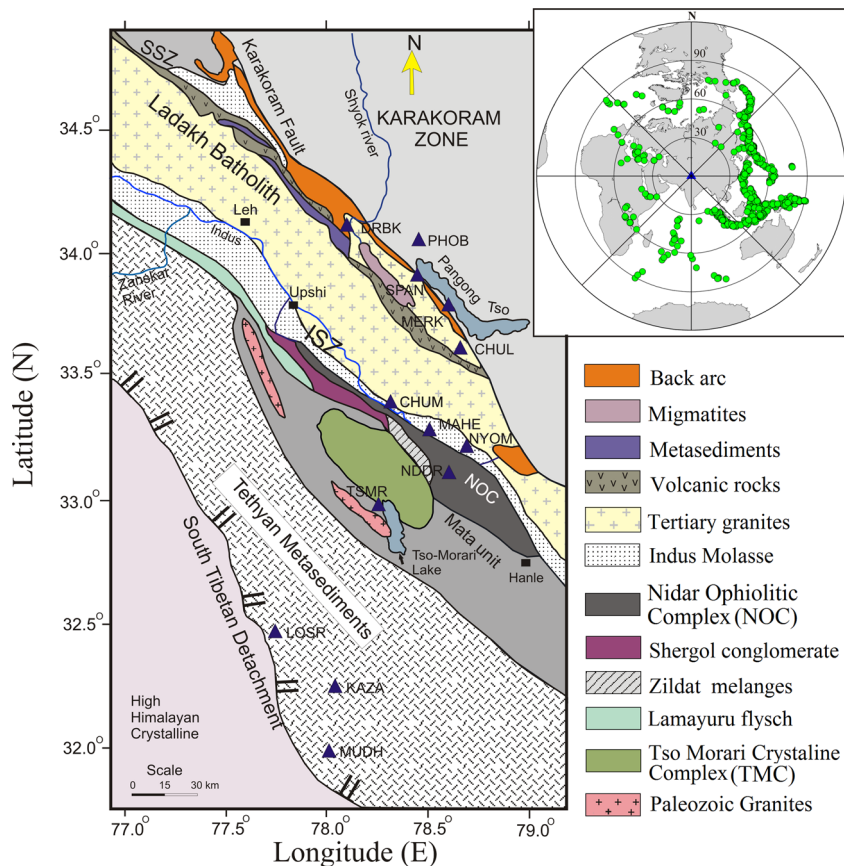


Figure 1. Simplified geological map of the study area showing parts of the Tethyan Himalaya, Indus suture zone (ISZ) and Karakoram zone (modified after Mahéo *et al.* 2004; Sen *et al.* 2013). The Shyok Suture Zone is indicated as SSZ. The seismological stations are shown by blue triangles. The inset shows distribution of teleseismic earthquakes (green filled circles) used for *P*-wave receiver function analysis.

Despite these compelling evidences of low shear wave velocity and low resistivity beneath Ladakh, the nature and geometry of intra crustal features are still poorly understood. Uncertainty still exists regarding the depth of Indian continental Moho beneath the TMC as well as the nature, depth and extent of the mid-crustal low velocity zone across the orogen (Caldwell *et al.* 2009; Rai *et al.* 2009). To address these issues, teleseismic receiver function study (Vinnik 1977; Langston 1979) has been carried out across the Tethyan Himalaya and eastern Ladakh covering the TMC, ISZ, Ladakh Batholith and Karakoram fault zone (Fig. 1). The objective of this study is to infer the distinctive features of the crust and characterize the IC-LVZ beneath the Tethyan and trans-Himalaya using receiver function analysis.

2 GEO-TECTONIC SETTING

The broad-band seismograph profile covers the major geo-tectonic units of the Tethyan and the trans-Himalaya of Himachal and eastern Ladakh region (Fig. 1). The Tethyan Himalaya is nearly 40–50 km wide and 3–5 km high, separated from the Trans-Himalayan range on the Tibetan block in the north by the Indus-Tsangpo Suture Zone (ITSZ; Gansser 1964). The Tethyan Himalaya exposes a continuous rock sequence ranging in age from the Proterozoic to Eocene and consists of siliciclastic and carbonate metasedimentary rocks interbedded with Paleozoic and Mesozoic volcanic sedimentary and metamorphic rocks (Thakur 1992; Srikantia & Bhargava 1998).

The Tethyan Himalaya shows a decreasing metamorphic grade from low grade meta-sediments at base to unmetamorphosed sediments upwards. The Tethyan Himalayan zone lies at the hanging wall of the South Tibetan Detachment (STD), which is a Cenozoic low angle normal fault that separates the Tethyan metasediments from the High Himalayan Crystallines. The TMC, the ISZ comprising of the Zildat Ophiolitic Mélange (ZOM) and Nidar Ophiolitic Complex (NOC), the Ladakh batholith and Karakoram zone are the significant tectonic units of eastern Ladakh region present from south to north (Fig. 1). The detailed geology of these tectonic units is discussed by Thakur & Misra (1984), Thakur (1992) and De Sigoyer *et al.* (1997). The TMC is a prominent litho-unit that lies on top of the north Indian continental margin, to the south of the ISZ (Fig. 1). In the northern extent, the TMC dips towards NE while in the southern extent it dips towards SW and therefore this region is referred as Tso-Morari dome. The TMC consists of ortho- and para-gneisses containing partly eclogitized metabasites enclaves and are intruded by granite. High pressure eclogite facies metamorphism has been observed in the TMC that suggests a deep subduction of the Indian Plate beneath the Eurasian Plate (Mukherjee & Sachan 2004). The Zildat fault separates the TMC to the north from the rock formations of the ISZ. The ISZ consists of Zildat Ophiolitic Mélange (ZOM) which is overlain by the Nidar ophiolites. The Nidar ophiolite extends along the ISZ and exhibits a complete cross section from upper mantle to supra ophiolitic sediments (Mahéo *et al.* 2004). The TMC and the ophiolites are well exposed in the Mahe valley as well as in the adjacent Nidar

valley of the study area (Fig. 1) and are separated by ZOM. The ZOM are meta-greywackes containing clasts of ophiolite, volcanics, chert and exotic carbonate blocks. Near the contact between TMC and ZOM, quartz veins are seen within the ZOM which are believed to have formed due to decompression melting of the TMC (Fig. 2a) (Sen *et al.* 2013). The ZOM and the ophiolites are characterized by presence of hydrous minerals like serpentine (Fig. 2b), talc and amphibole, etc. In Mahe valley the gabbroic crustal part of the ophiolites has a contact with serpentinized peridotites (Fig. 2c), which is the upper most part of mantle ultramafics of the ophiolite. The contact is identified as petrologic Moho within the NOC. It occurs as a 500-m-thick zone having repeated intercalation of gabbro and serpentinites. In the adjacent Nidar valley (Fig. 1) the mélange is completely absent. The TMC has a north dipping contact with the mantle section of the ophiolite suite. The bottom of the mantle section is occupied by a dunite body (~ 3 km thick). This dunite body is essentially composed of olivine along with disseminated spinel and layered chromites (Fig. 2d). Serpentization is heterogeneous, often fracture controlled and varies from 10 to 80 per cent; in places the ultramafics are entirely serpentinized around the contact. The serpentines may be considered as an evidence for hydration of the mantle wedge above subduction zones. Generally spinel peridotites originate at <60 km depth (<2 GPa) (Coleman 1977). So the contact between the TMC and dunite may exist up to ~ 50 km depth. The Ladakh batholith is located north of the ISZ which is bounded to the north by the Khardung back arc volcanics and the Shyok Suture Zone. The Ladakh batholith is a magmatic arc constituted of granite with minor rhyolites to andesites forming Andean-type calc-alkaline magmatism generated by subduction of the Neo-Tethys oceanic plate under the Eurasian continental plate

during Early Cretaceous to Late Eocene periods (Schärer *et al.* 1984; Weinberg & Dunlap 2000; Sen & Collins 2013). The region south of this magmatic arc (i.e. ISZ and TMC zone) is known as forearc region. The Shyok Suture zone lies between Ladakh batholith and Karakoram zone extending in a NW–SE trending belt into eastern Ladakh. The back arc region is recognized just north of Ladakh batholiths as shown in Fig. 1. The rocks overlying the Shyok suture zone separated by the north dipping Karakoram fault are grouped under Karakoram zone, which consists of metapelites, migmatites, granodiorites and leucogranites.

3 SEISMOLOGICAL PROFILE AND DATA

The dataset is composed of waveforms of teleseismic earthquakes recorded by three broad-band seismological stations (MUDH, KAZA and LOSR) of Kinnaur network, Himachal Pradesh (Hazarika *et al.* 2013) and 10 stations of Ladakh seismological network operated by Wadia Institute of Himalayan Geology, Dehradun (Fig. 1). The seismological stations of Kinnaur Network recorded about 200 teleseismic earthquakes during 2008–2010. The Ladakh seismological stations recorded about 600 teleseismic earthquakes during 2009–2011. All the seismological stations were equipped with Trillium 240 seismometer with a flat velocity response for the frequency range of 0.004–35 Hz. Taurus data logger with dynamic range >138 dB (Make M/S Nanometrics, Canada) and 40 GB storage capacity hard disk were used for data storage that enable continuous recording at remote stand-alone stations for a longer time period. The recording sampling rates of Kinnaur and Ladakh

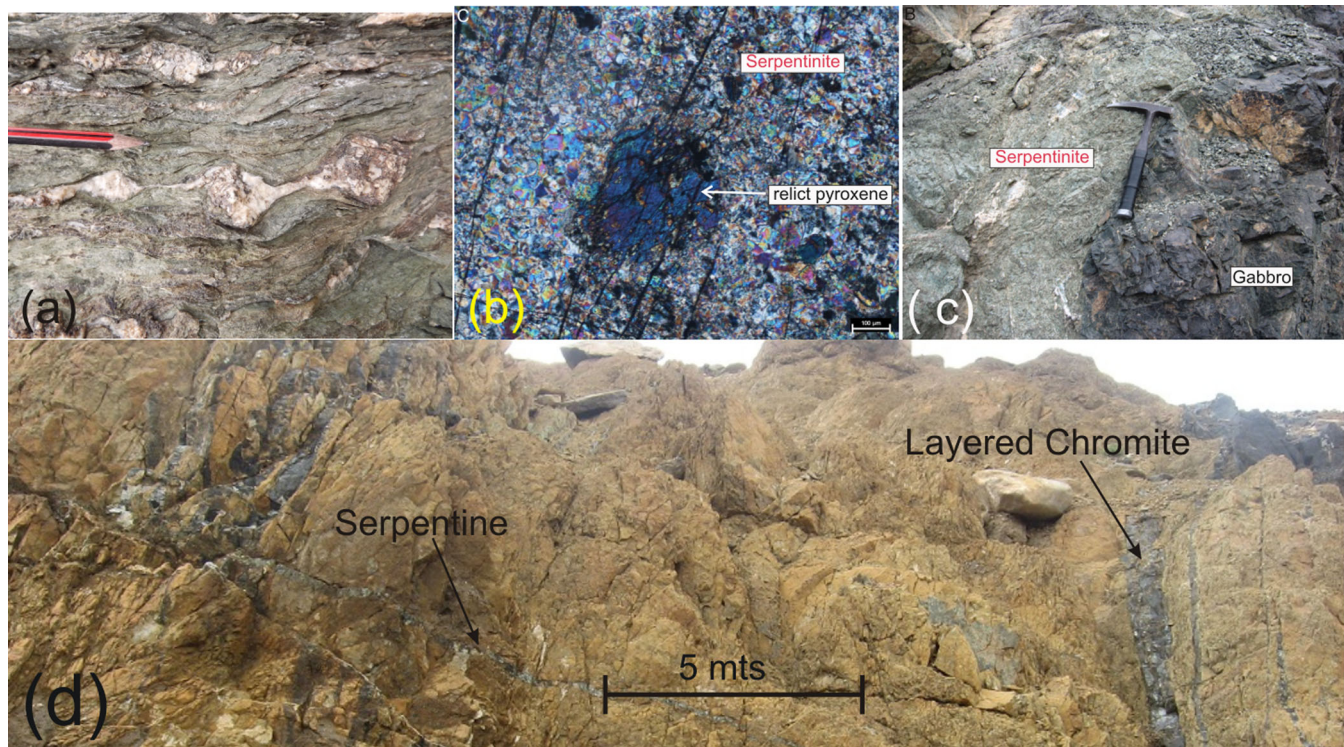


Figure 2. Field and microscopic features as evidences of serpentinization/hydration/partial melting from the study area showing (a) mylonitized quartz veins within the ZOM, adjacent to the TMC. This quartz veins are silica-rich fluids that formed due to decompression melting of the TMC. (b) Photomicrograph (cross Nicol) of serpentinized peridotites showing almost complete serpentinization with relict pyroxene of the peridotites. (c) Field photograph showing contact between serpentinized peridotites and gabbro in Mahe valley. (d) Spinel bearing serpentized Dunite in Nidar valley showing presence of serpentine and chromite veins.

seismological stations are 100 and 20 samples per second (SPS), respectively. The timing of the digitizer was synchronized with Global Positioning System (GPS) receivers. The waveform data are selected based on the following criteria: (1) body-wave magnitude $m_b > 5.5$ to favour high signal-to-noise ratio, (2) epicentral distances (Δ) within 30° and 90° to avoid wavefield complexities due to upper-mantle discontinuities. Information for teleseismic earthquakes is extracted from PDE catalogue of U.S. Geological Survey (<http://neic.usgs.gov>). The geographical distribution of epicentres of the earthquakes selected for the study is shown in Fig. 1(inset). The seismological profile recorded majority of earthquakes from the Circum-Pacific seismogenic belt. The azimuthal distribution of earthquakes are similar to those reported by other studies in Himalayan region (Hazarika *et al.* 2012; Hazarika *et al.* 2013). However, sufficient teleseismic earthquakes were also recorded from other backazimuths (BAZ) that helped to examine the azimuthal variation of crustal structure.

The three seismological stations of Kinnair network, for example Losser (LOSR), Mudh (MUDH) and Kaza (KAZA) are located over the Tethyan Himalaya. The data of 10 broad-band seismological stations of Ladakh network mostly sample the eastern part of Ladakh region (Fig. 1). The southernmost station of the profile, Tso-Morari (TSMR) station, lies on the TMC; Nidar (NDDR) lies over the NOC; Nyoma (NYOM) and Mahe (MAHE) are on eastern end of the ZOM (Thakur & Virdi 1979; Thakur & Misra 1984). The Chumathang (CHUM) and Chushul (CHUL) stations lie over the Indus molasse and the Ladakh batholith (Thakur & Misra 1984), respectively. Merak (MERK) and Spangmik (SPAN) stations lie over the backarc region; Phobrang (PHOB) and Durbuk (DRBK) stations are located over the Karakoram fault zone (Thakur & Mishra 1984).

4 METHODOLOGY

4.1 RF analysis

The P -wave receiver function analysis is a widely used technique for determination of crustal structure beneath a single seismological station (Vinnik 1977; Langston 1979). The RFs are computed by deconvolving the vertical component of a seismogram from radial and tangential components resulting radial and tangential RFs. The deconvolution process removes the source and path effects contained in the teleseismic P -waveform and only P -to- S (Ps) converted waves produced by large velocity contrasts as well as their reverberations remain in the source equalized P -wave train. The Ps converted phases and their reverberations are clearly observed in the radial RF. Modelling of the amplitude and timing of these phases provide constraints on the underlying discontinuities (Owens *et al.* 1984; Ammon *et al.* 1990). Prior to RF computation using deconvolution algorithm, the original waveforms are pre-processed by windowing the data to include no more than 60 s before and 100 s after the P -wave arrival, re-sampling the waveform data to 10 SPS, filtering the waveforms using a Butterworth bandpass (filter range 0.01–4.0 Hz) and rotation into ZRT (vertical, radial and transverse) system. We have applied iterative time domain deconvolution technique of Ligorria & Ammon (1999) for computation RFs. During computation of RF, a Gaussian filter is used with Gaussian width 1.5. The RFs with good SNR and more than 80 per cent waveform fit are used for further analysis.

To illustrate the adopted methodology, the RF analysis at MAHE seismic station is discussed (Figs 1 and 3). This station recorded about 600 teleseismic earthquakes from a wide range of backaz-

imaths (~ 20 – 337°) (Fig. 1, inset). Examples of individual radial RFs are plotted as a function of backazimuth (Fig. 3a) which shows strong azimuthal variation of different phase arrivals. For simplicity the RFs of the earthquakes arriving from NE, SE, SW and NW are named hereafter as NE, SE, SW and NW group, respectively. The individual RFs show strong positive arrivals at ~ 9.0 s for the earthquakes of NE, SW and NW groups; whereas, this phase is not clearly observed in SE group. This distinctive feature is also clearly shown in the stacked RFs of SE and NE group (Figs 3b and c). Based on polarity, arrival time and also from the previous RF study (Rai *et al.* 2006), this phase (Ps_2) is considered as converted phase originated from the Indian Moho. Prior to this Ps_2 phase, another strong positive arrival is observed at ~ 6.5 s (marked as Ps_1 phase in Fig. 3c). Besides these positive arrivals, negative arrival at ~ 2.0 and ~ 4.0 s is also observed. Based on polarity and arrival time, the positive and negative arrival at ~ 30 and 38 s observed in NE group of RF is identified as crustal multiples ($PpPms$ and $PpSms + PsPms$ arrivals) originated due to reverberation of Moho converted Ps_2 phase (Fig. 3c). Likewise, the positive and negative arrival at ~ 20 and 22 s is considered as reverberation of converted phase Ps_1 (Fig. 3c). The sources of the converted phases (Ps_1 and Ps_2) are discussed in the succeeding sections.

4.2 H-K stacking analysis

The thickness (H) of converting layers in the crust and corresponding average Vp/Vs ratio can be estimated from relative timing of P -to- S conversion and its reverberations following Zhu & Kanamori (2000). The time difference between direct P -arrival (Pp) and converted phases (Ps_1 and Ps_2) largely depend on thickness of the converting layers and Vp/Vs ratios. The Vp/Vs ratio is related to Poisson's ratio (σ) by the relation $\sigma = 0.5 \times [1 - 1/(k^2 - 1)]$, where $k = Vp/Vs$. The $PpPms - Ps$ and $(PpSms + PsPms) - Pp$ times are two way travel time of S and P waves, respectively and their ratio is proportional to Vp/Vs ratio (or Poisson's ratio) and crustal thickness (Zandt & Ammon 1995; Zhu & Kanamori 2000). Here we extend the single-layer approximation of Zhu & Kanamori (2000) to a three-layer crustal model (as described in Tang *et al.* 2008) for careful delineation of discontinuities as indicated by presence of Ps_1 and Ps_2 phases observed at the stations located close to the ISZ. The weighting factors considered for Ps , $PpPms$, and $PpSms + PsPms$ phases are 0.7, 0.2 and 0.1, respectively. The average crustal P -wave velocity for upper crust and whole crust have been used from Oreshin *et al.* (2008). The Ps_1 and Ps_2 phases and their multiples allow us to differentiate the Poisson's ratio of upper crust from the average Poisson's ratio estimated for the whole crust. The RF stacking procedure is illustrated using NE group of RFs showing clear Ps_1 and Ps_2 phases recorded at MAHE seismic station (Fig. 4). The best estimated H and k values are indicated by the centre of the error ellipse (marked by star) calculated following Zhu & Kanamori (2000). A grid search over a wide range of H and Vp/Vs (or σ) values shows two sets of optimal values ($H_1 = 45.9$ km, $\sigma_1 = 0.316$) and ($H_2 = 75$ km, $\sigma_2 = 0.280$) that maximize the summation of amplitudes of the converted and multiple phases (Fig. 4). Ellipse surrounding the star represents depth and Vp/Vs ratio of strongest P -to- S conversion with error. These two optimal values indicate two velocity discontinuities corresponding to two strong converted phases, that is Ps_1 and Ps_2 . The Poisson's ratio of the upper crust is much higher ($\sigma_1 = 0.316$) than average crustal Poisson's ratio ($\sigma_2 = 0.280$). Similar analysis has been carried out for other selected stations that show clear record of Ps_1 and Ps_2 .

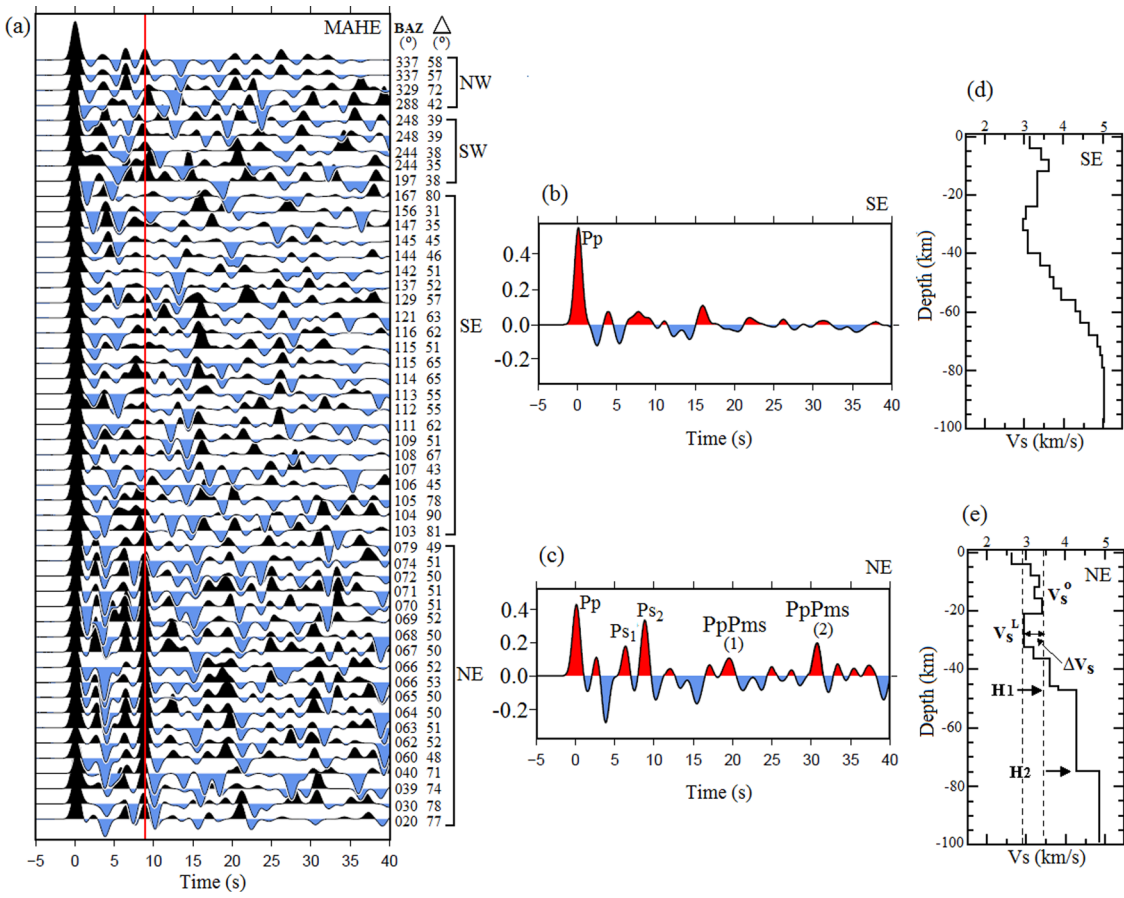


Figure 3. Plots of (a) individual RFs as a function of backazimuth (BAZ) after distance moveout correction for the P_s phase to a reference distance of 67° and slowness 6.4 s deg^{-1} . The stacked RFs of SE and NE group are shown in (b) and (c). The inverted shear wave velocity models of depth section up to 100 km obtained from SE and NE group of RFs are shown in (d) and (e). The H1 and H2 are two layers observed in (e) with step jump in velocity responsible for generation of P_{s1} and P_{s2} phases. For estimation of degree of velocity reduction, the upper-crustal velocity peak (V_s^0) is marked by dashed lines in (e), which is considered as an estimate of the velocity of unperturbed crust and the minimum velocity in the IC-LVZ is marked as V_s^L . The percentage of velocity reduction is estimated from V_s^0 and V_s^L . The minimum velocity beneath MAHE shows a V_s reduction (ΔV_s) of 17.64 per cent.

4.3 RF modelling

The shear wave velocity (V_s) structure beneath all the stations of the profile is estimated applying the least-squares inversion method of Ammon *et al.* (1990). The method is illustrated using RFs of NE group recorded at MAHE station. The individual RFs are stacked (black waveform in Fig. 5c) and ± 1 standard deviation (SD) bounds are calculated (grey-shaded area in Figs 5b and c) which are used for constraining the inverted models. The inversion scheme needs a starting velocity model close to true earth velocity structure which is defined based on previous study (Rai *et al.* 2006; Oreshin *et al.* 2008). The starting model is perturbed moving the interfaces up and down within a reasonable range of depth of 1 km interval using perturbation scheme as described in Ammon *et al.* (1990). This perturbation scheme gives a set of new starting models (Fig. 5a), allowing the exploration of a wide initial model space and reducing the dependence of the solutions on the starting model. The perturbation scheme produces about 300 initial models. The stacked RF of the given station is inverted by minimizing the difference between the observed and synthetic RFs computed for all the initial models produced by the perturbation scheme and simultaneously constraining the model smoothness (Ammon *et al.* 1990). The velocity models that produce synthetic RFs falling within $\pm 1 SD$ bounds are shown

in Fig. 5(b) (black waveforms). One of the best-fitted models is selected and the thin layers with similar velocities are grouped into a single layer so as to derive the main features of the structure. The simplified model is again used as starting model and the inversion procedure is repeated until the dominant phases are modelled avoiding the over complexities in the resultant model. The synthetic RFs are computed using reflectivity method (Kennett 1983). The synthetic seismogram (red waveform) corresponding to final velocity model is compared with stacked RF (black waveform) in Fig. 5(c). The representative best-fitting inverted models (thin black line) as well as simplified final velocity model (thick black line) are shown in Fig. 5(d).

The modelling at MAHE station shows S -wave velocity of 2.6 km s^{-1} in the uppermost surface which increases to about 3.4 km s^{-1} within the depth range $\sim 7\text{--}20 \text{ km}$. An IC-LVZ ($V_s: \sim 2.8 \text{ km s}^{-1}$) is observed at $\sim 20\text{--}36 \text{ km}$ depth. The V_s increases to ~ 4.2 and 4.8 km s^{-1} at the depths of ~ 46 and $\sim 75 \text{ km}$ (Fig. 5). The step jump in velocity at $\sim 75 \text{ km}$ may indicate the Indian Moho. Modelling of RF of SE group also shows similar structure, but the step velocity jump at $\sim 75 \text{ km}$ is absent (Fig. 3d). In order to understand nature of the low velocity zone, the degree of velocity reduction is estimated using the upper-crustal velocity peak, which is considered as an estimate of the velocity of unperturbed crust

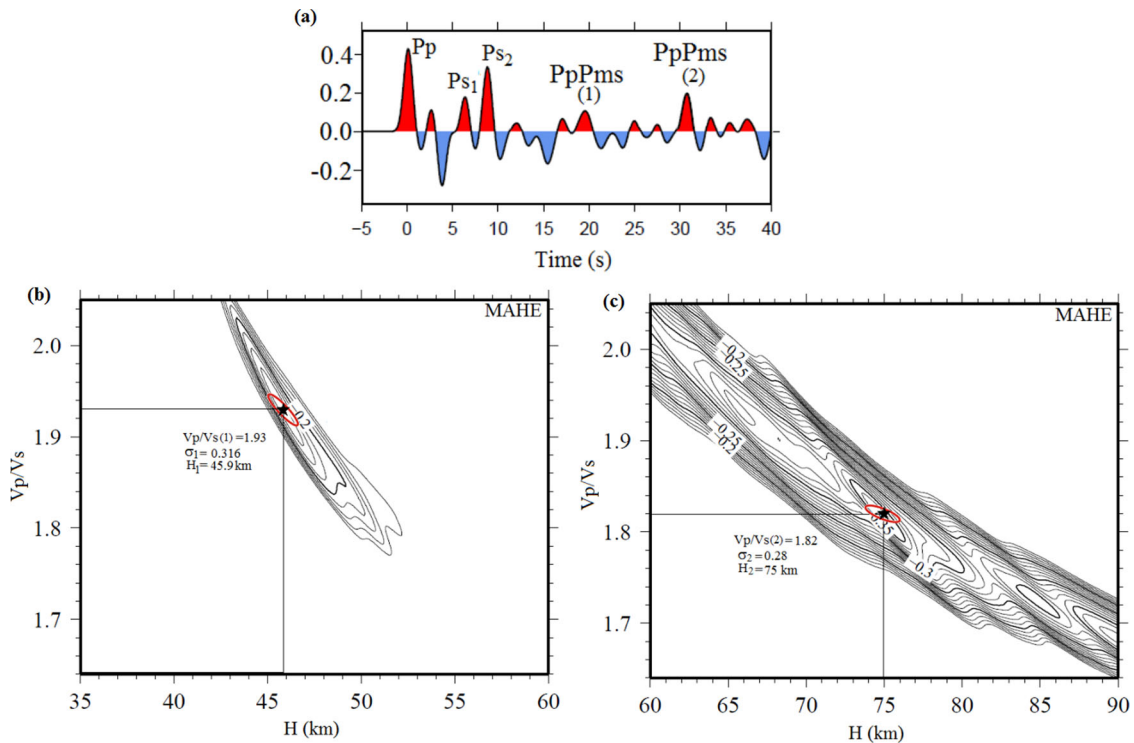


Figure 4. Figure showing results of H - K stacking analysis of NE group of earthquakes recorded at MAHE seismological station. The stacked RF of NE group is shown in (a) and results of H - K stacking analysis using Ps_1 and Ps_2 phases and their multiples are shown in (b) and (c), respectively. The Poisson's ratio is observed to be higher ($\sigma_1 = 0.316$) in the upper crust above mid-crustal layer ($H_1 = 45.6$ km) compared to that observed for the whole crust ($\sigma_1 = 0.280$) above Moho depth ($H_2 = 75$ km).

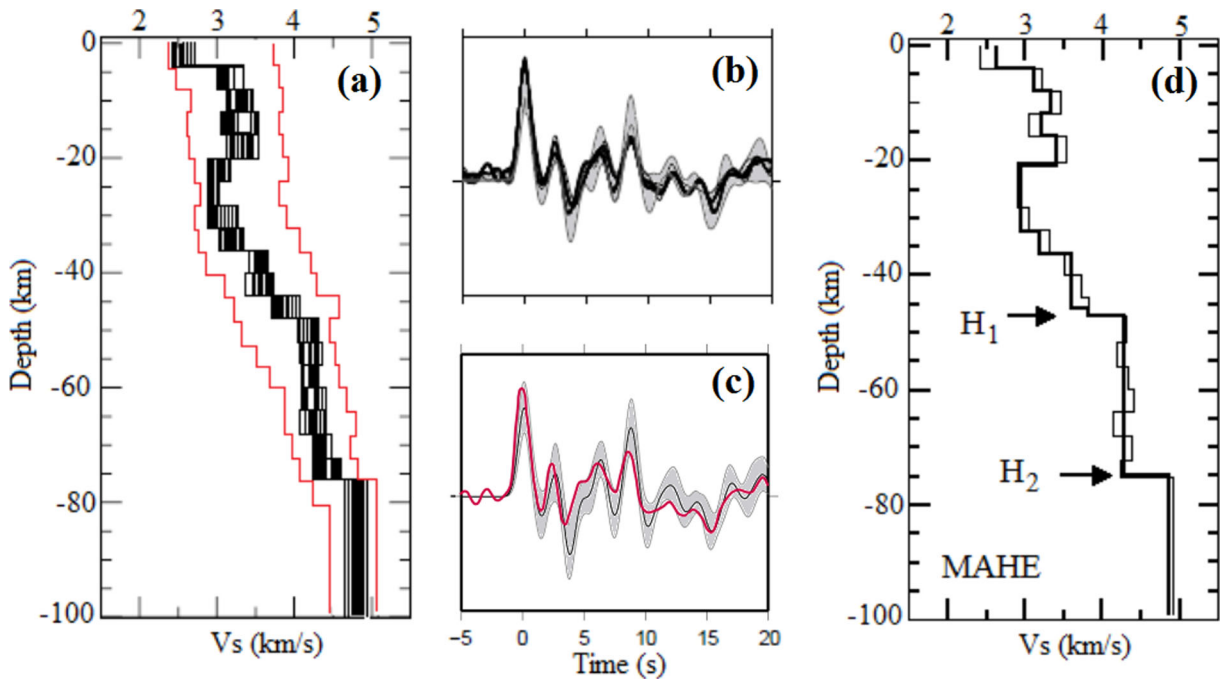


Figure 5. Inversion results of MAHE receiver functions. The inverted velocity models are shown on the left (a) as black solid lines where the range of starting models is indicated by red lines. The synthetic receiver functions corresponding to the range of inverted models in 'a' are shown in the middle panel (black waveforms) (b), the grey-shaded area shows ± 1 SD bound of observed receiver functions. The synthetic (red) receiver function and stacked RF (black waveform) is shown with $\pm SD$ bounds in panel (c) along with corresponding stacked tangential receiver function shown below it. The representative best-fitting inverted (thin black line) as well as simplified final velocity model (thick black line) are shown in the right-hand panel (d). The mid-crustal layer (H_1) and Moho discontinuity (H_2) is marked by arrows in 'd'.

(marked as V_s^0 shown by dashed lines in Fig. 3e) and the velocity in the IC-LVZ is marked as V_s^L . The minimum velocity beneath MAHE shows a V_s reduction (ΔV_s) of 17.64 per cent. The above methodology is used for the rest of the stations of the profile.

5 RESULTS

5.1 Azimuthal variation of crustal converted phases

The RFs at each station have been computed using the method described above. The seismic stations of the profile recorded teleseismic earthquakes arriving from wide range of backazimuth that facilitates studying azimuthal variation of crustal structure (Fig. 1, inset). The individual RFs at each station are plotted as a function of backazimuth (examples are shown in Figs 6 and S1). The individual RFs observed at stations of Kinnaur network shows consistent arrival of Moho converted P_s phase irrespective of azimuth of the earthquakes, whereas a common feature in the RF of Ladakh seismological stations is the variation of converted phases, both in amplitude and sharpness, for earthquakes arriving from different azimuths. At the southern most station of the profile (TSMR station), the RFs of earthquakes arriving from SE to SW (BAZ: 83°–146°) show a positive arrival around 9 s (Fig. 6a). This phase at ~9 s is not observed for earthquakes arriving from NE and NW. On the other hand, the RFs of NE and SE group show a positive arrival at ~13 s whereas SW and NW group of RFs show a positive arrival at ~15 s. The varied phase arrivals from different BAZ at different times suggest strong azimuthal variation beneath the TSMR station. Similar azimuthal variation is also observed at stations located close to the ISZ (e.g. NDDR, NYOM, MAHE and CHUM). Example of RFs of NDDR station is shown in Fig. 6(b). The RFs of the earthquakes arriving from SE do not show clear P_s converted phase whereas it is clearly identified for the earthquakes from other BAZ at around 9 s (Fig. 6b). On the contrary, the seismic station close to Pangong Tso region (e.g. MERK) shows clear and consistent P_s phase at around 10.5 s for the earthquakes arriving from NE as well as SE (BAZ: ~30°–146°; Fig. 6c). At the northern most stations of the profile (DRBK, SPAN and PHOB), the P_s phase is consistently observed within ~9.5–10 s for earthquakes arriving from all BAZ except for few earthquakes of NW group (RFs of PHOB is shown in Fig. 6d as an example).

The azimuthal variation at each station is critically examined estimating ray piercing points of the teleseismic waves at the depth of Moho. The ray piercing points are calculated by ray tracing the incident Moho converted P_s phase through the crust, using the ray parameter calculated from the focal depth and epicentral distance of the earthquake. The IASP91 global velocity model (Kennett & Engdahl 1991) has been used for calculation of piercing points. Example of ray piercing points corresponding to RFs of five representative stations (Figs 3 and 6) is shown in Fig. 7. The piercing points shown by open symbols indicate absence of clear Moho converted P_s phase (or P_{s2}). The piercing points shown by grey filled symbols and black filled symbols indicate clear record of only P_{s2} phase and clear record of both P_{s1} and P_{s2} phases, respectively. It is observed from the ray piercing points and strength of corresponding P_s phase that, regardless of backazimuth, when the rays pierce some part of the ISZ, the Moho converted P_s phase is not clearly seen. Typical examples of ray piercing points corresponding to RFs of MAHE (Fig. 3a) and NDDR (Fig. 6b) station located over ISZ are shown in Fig. 7. In both the stations, the RFs of SE group do not show clear P_s phase as the rays pierce by and large the

NOC and TMC region whereas earthquakes from NE group mostly shuttle the Ladakh batholith and Karakoram zone showing clear P_s phase. At the stations towards north of the profile (e.g. PHOB, DRBK stations), the NE as well as the SE group of earthquakes pierce the Karakoram zone and the SW group pierce the Ladakh batholith showing clear P_s phase whereas few RFs of the NW group do not show clear P_s phase that pierces the Karakoram fault zone. The analysis of strength of individual P_s phase and its corresponding ray piercing point enables us to demarcate the region having complexity in the crust-mantle boundary.

5.2 Shear wave velocity structure beneath the profile

In order to track the geometry of Moho and intracrustal features along the profile, we plotted selected RFs that show clear Moho converted P_{s2} phases presumably based on prior geological knowledge (Fig. 8). Moreover, in case of the stations close to suture zone, only those RFs are selected and plotted in Fig. 8 that show clear P_{s1} and P_{s2} phases. In all the stations, a strongest positive arrival is observed after the direct P -wave (marked by yellow lines in Fig. 8) arrival which is laterally continuous interface along the profile except small part close to the ISZ. The delay time of P_{s2} phase with respect to direct P -arrival estimated at each station varies within the range ~7.5–10 s. This phase is considered as the Moho discontinuity of the underthrusting Indian Plate. The delay time of this phase is ~7.5 s for KAZA, LOSR and MUDH stations. The delay time of P_{s2} phase at TSMR is ~9 s which gradually increases up to ~10 s at MERK and SPAN station. At TSMR station the P_{s2} phase is comparatively weak. The PHOB and DRBK stations lying to the west of the profile show ~9.5 and 9 s delay time, respectively. In addition to this strong positive arrival at ~9–10 s observed north of the ISZ, another strong positive arrival is consistently observed at around 6.5 s at stations NDDR, NYOM, MAHE, CHUM, CHUL and MERK. One more prominent feature in the RFs of all the stations is the significant negative arrivals after the direct P arrival (within time window 2–4 s). These negative amplitudes observed in all the stations may be the converted phases at an interface with negative velocity gradient and indicate the presence of intrarustal low velocity zone (IC-LVZ). The successive negative amplitudes may be the free multiples originated at the top of the IC-LVZ.

The stacked RFs at each station (red waveforms, shown in top panel of Fig. 8) are used for modelling shear wave velocity structure shown in the lower panel. The Moho discontinuity of the underthrusting Indian Plate is identified as the depth where there is a sharp step velocity jump attaining at least 4.5 km s^{-1} value of shear wave velocity for the mantle. However, at TSMR station located over TMC, it is marked by gradational velocity transition over a thickness of ~20 km with typical mantle velocity of $>4.6 \text{ km s}^{-1}$. In this station, the velocity in the lower crust is higher (~ 4.4 km s^{-1}) compared to the rest of the stations of the profile. The inverted velocity models at MUDH, LOSR and KAZA stations lying over the Tethyan Himalaya show ~60-km-thick crust. In eastern Ladakh, the inverted velocity models show a progressive deepening of the Moho from ~75 km at TSMR to ~80 km beneath MERK and SPAN. However, the stations lying further northwest of the profile (e.g. PHOB and DRBK) again show thinner crust (~75 km thick). The seismological station to the north of the NS profile (e.g. DRBK, PHOB, SPAN, MERK and CHUL) follows SE dipping trend and the estimated crustal thickness suggests the Moho as NW–SE dipping interface underneath Ladakh batholith. In addition to Moho, velocity models obtained at NDDR, NYOM, MAHE, CHUM and MERK

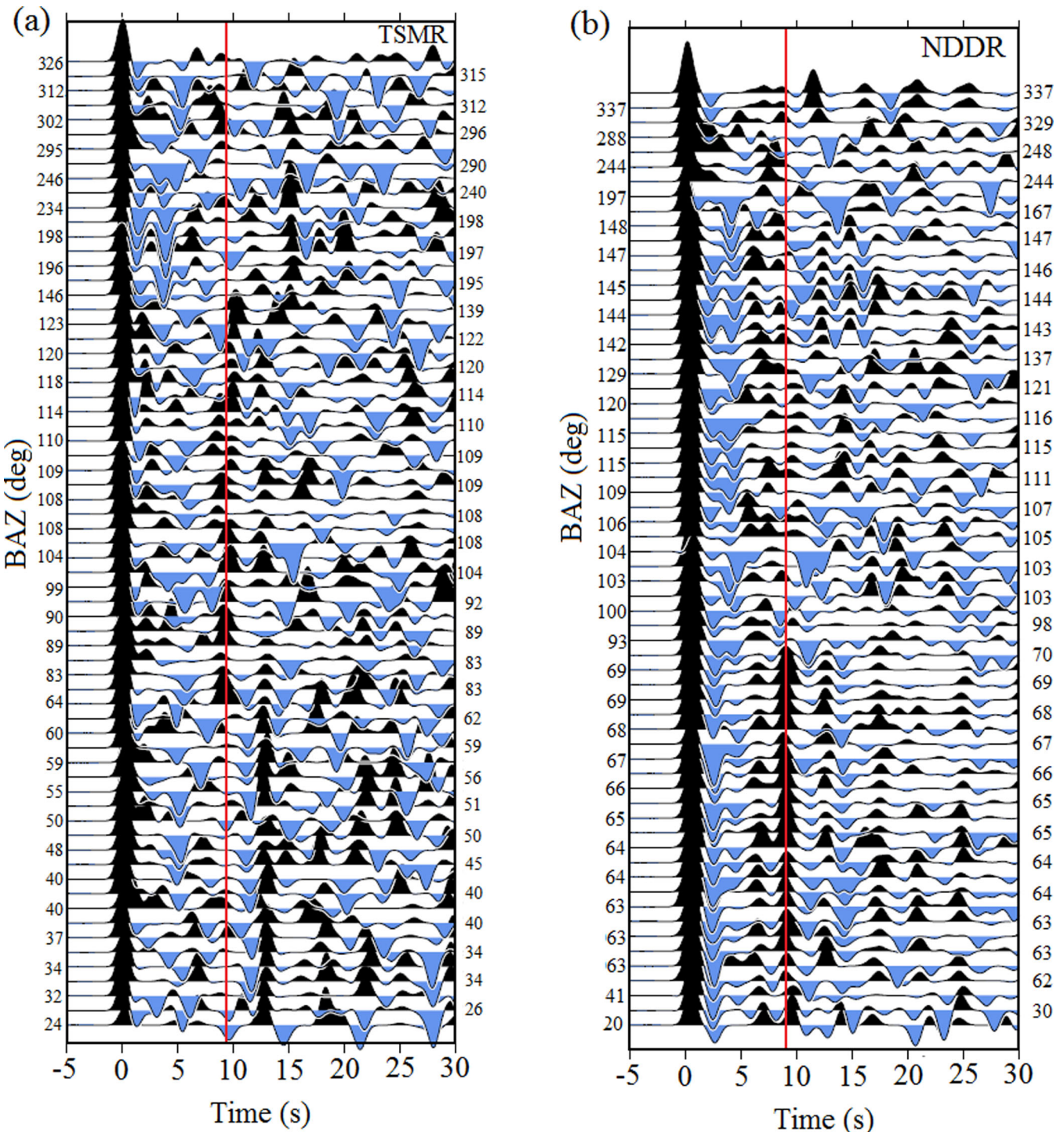


Figure 6. Examples of receiver functions plotted as a function of backazimuth recorded at seismological stations (a) TSMR, (b) NDDR, (c) MERK and (d) PHOB. The RFs at each station show strong azimuthal variation. The ray piercing points of corresponding P_s converted phases at Moho are shown in Fig. 7.

stations clearly show another velocity discontinuity at $\sim 47\text{--}50\text{ km}$ depth. This layer corresponds to P_{s1} phase observed at $\sim 6.5\text{ s}$, which is as prominent as the Moho converted P_{s2} phase (Fig. 8). The inverted velocity model at each station shows a pronounced IC-LVZ at mid-crustal depth (shown by grey shaded area in Fig. 8, lower panel). The decrease in velocities at these stations starts at depths of $\sim 15\text{--}20\text{ km}$ and that goes up to $\sim 30\text{--}40\text{ km}$. The minimum S -wave velocities at IC-LVZ range between 2.7 and 3.0 km s^{-1} .

The S -wave velocities are much lower ($\sim 2.7\text{--}2.8\text{ km s}^{-1}$) beneath the stations close to ISZ (e.g. TSMR, NDDR, NYOM and MAHE) compared to stations towards north and south. The percentage of velocity reduction relative to average velocity of the upper crust is estimated at each station. The stations beneath the Tethyan Himalaya show $\sim 8.5\text{--}11.4$ per cent velocity reduction whereas the velocity reduction attains maximum beneath Ladakh seismological stations ($\sim 16\text{--}19$ per cent).

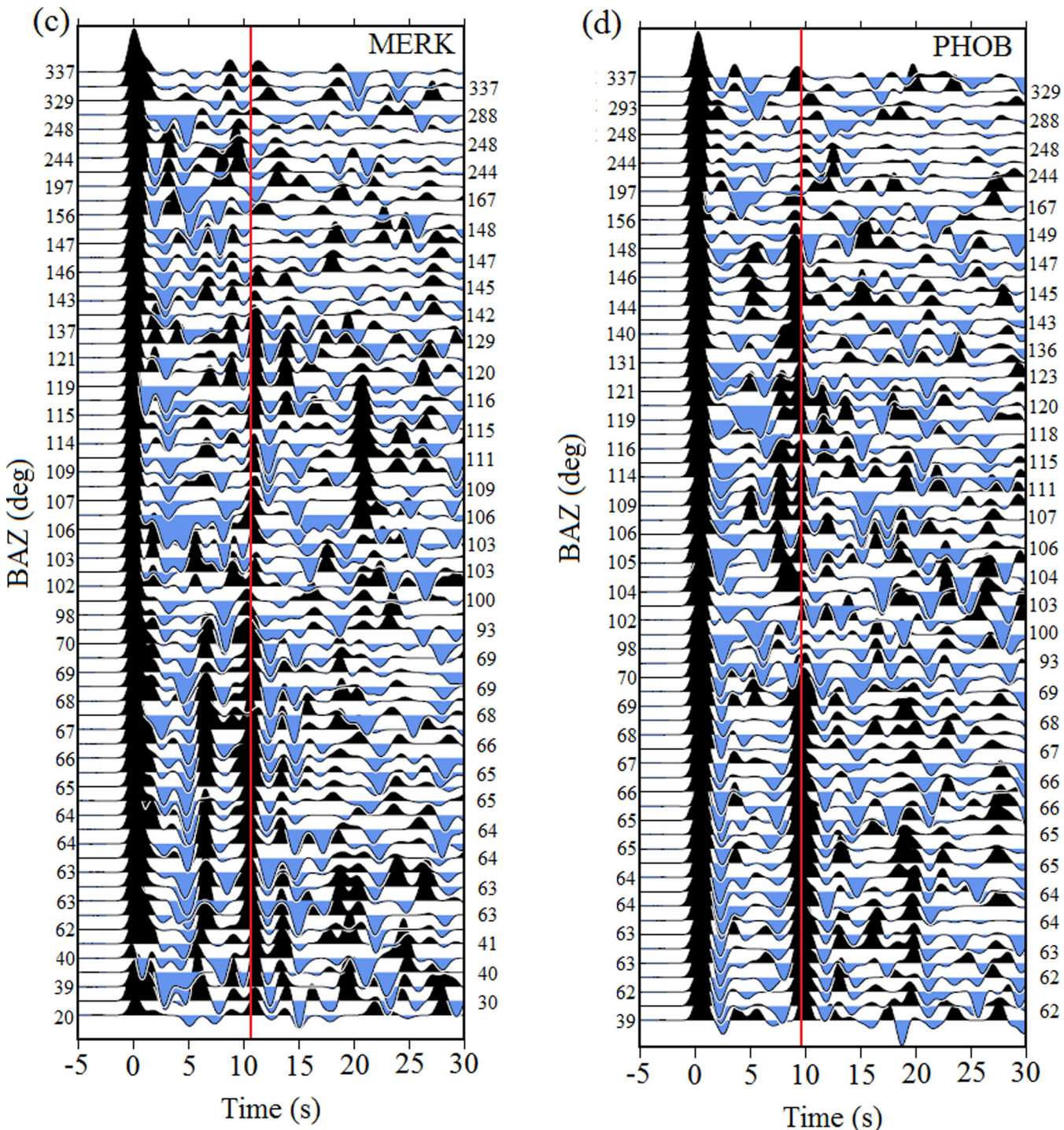


Figure 6. (Continued.)

5.3 Poisson's ratio estimations

The average Poisson's ratios of the crust beneath each station of the profile were estimated earlier by Hazarika *et al.* (2013). We extended this study by analysing additional data recorded at six seismic stations (e.g. NDDR, NYOM, MAHE, CHUM, CHUL and MERK) during 2009–2011 using the methodology illustrated in the Section 4.2. These six stations are selected based on clear record of two crustal converted phases (P_{S1} and P_{S2}) originated due to a mid-crustal layer and Moho respectively (Fig. 8). Analysis of

these two converted phases permits us to estimate Poisson's ratio in the upper crust (using P_{S1} phase and its multiples) as well as average Poisson's ratio of the entire crust (using P_{S2} phase and its multiples) separately. The results are listed in Table 1. The analysis shows that Poisson's ratio in the upper-middle crust (above $\sim 47\text{--}50\text{ km}$) is usually higher compared to average Poisson's ratio of the entire crust at each station. Moreover, by comparing upper-crustal Poisson's ratios among the stations, it is observed that Poisson's ratio is higher (≥ 0.30) beneath NDDR, NYOM, MAHE, CHUM stations located close to forearc region compared to the values

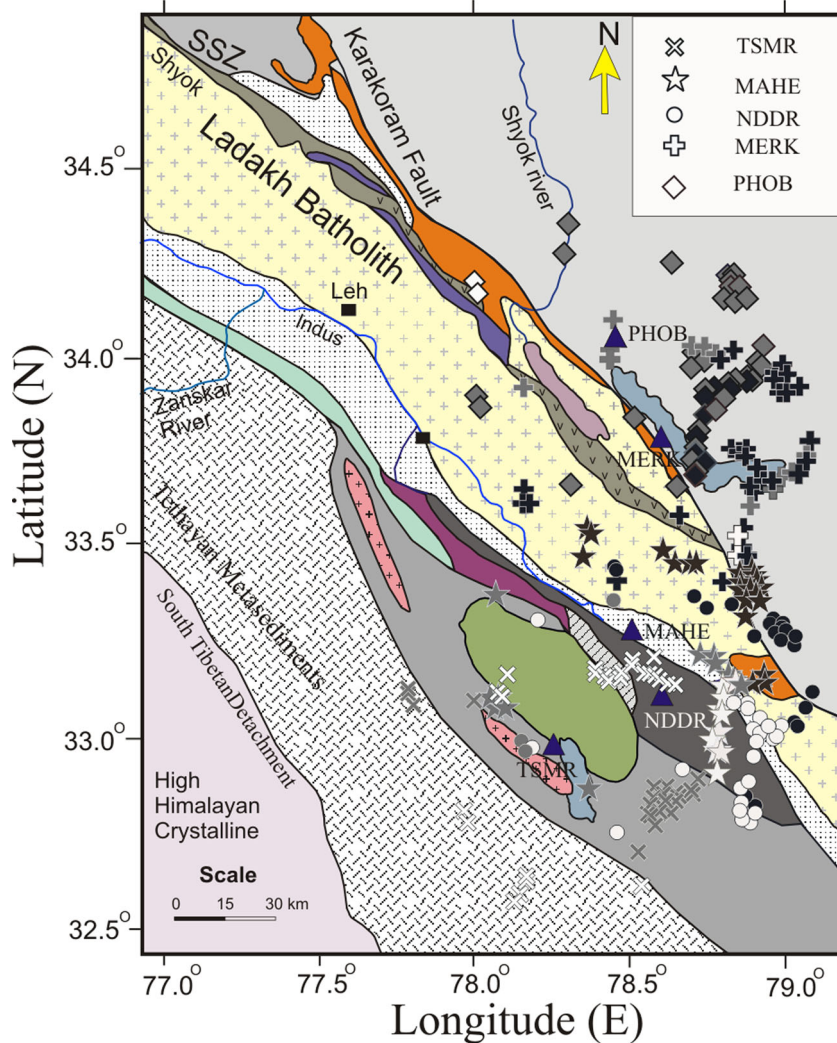


Figure 7. Ray piercing point analysis computed at five representative stations (e.g. TSMR, MAHE, NDDR, MERK and PHOB). The piercing points corresponding to each recording station are shown by different symbols. The piercing points shown by open symbols indicate absence of clear Moho converted P_s phase (or P_{s2}). The piercing points shown by grey filled symbols indicate clear record of only P_{s2} phase whereas black filled symbols indicate presence of both P_{s1} and P_{s2} phases.

observed at CHUM and MERK stations located in the northern part of Ladakh batholith.

6 DISCUSSION

Numerous receiver function analyses have been carried out in the Himalaya and Tibet in the past by the INDEPTH program (Phase I, II and III). The crust and mantle structure beneath the Himalaya and the Tibetan plateau owing to Indo-Eurasian continental collision have been well documented by INDEPTH and other related studies (Kind *et al.* 2002; Wittlinger *et al.* 2004; Schulte-Pelkum *et al.* 2005; Kumar *et al.* 2006a,b; Rai *et al.* 2006; Nábělek *et al.* 2009; Zhao *et al.* 2010, 2011). However, these studies emphasized more on the major discontinuities, especially the nature and depth of the Moho and the extent of the underthrusting Indian Plate beneath Tibet. In this study, we have stressed on the intracrustal structures and subsurface lithology of the Indo-Eurasian collisional suture zone. The major inferences of our study are discussed in the following sections.

6.1 Variation of crustal thickness

The strongest positive arrival after the direct P wave is considered as Moho converted P_s phase (P_{s2}) which is observed at ~ 7.5 s beneath the Tethyan Himalaya. It varies within ~ 9 – 10 s beneath Ladakh. The inversion of RFs at each station suggests variation of crustal thickness from ~ 60 km beneath Tethyan Himalaya to ~ 80 km beneath Ladakh (Fig. 8). This observation agrees with the previous seismological (Rai *et al.* 2006; Oreshin *et al.* 2008, 2011; Hazarika *et al.* 2013) and gravity studies (Chamoli *et al.* 2011) obtained for this part of India–Asia collision zone. Recent study by Li *et al.* (2014) also suggests progressive thickening of crust towards north. The shear wave velocities in the velocity models (Fig. 8, lower panel) agree with the previous studies with some difference in upper-mantle velocities. The modelling technique using P -wave RF does not have much control on upper-mantle velocity. The increase in crustal thickness from south to north indicates the underthrusting of the Indian Plate beneath the Eurasian Plate. Comparing the crustal thicknesses obtained from passive source seismological study along the HIMPROBE profile (Rai *et al.* 2006; Oreshin *et al.* 2008) and

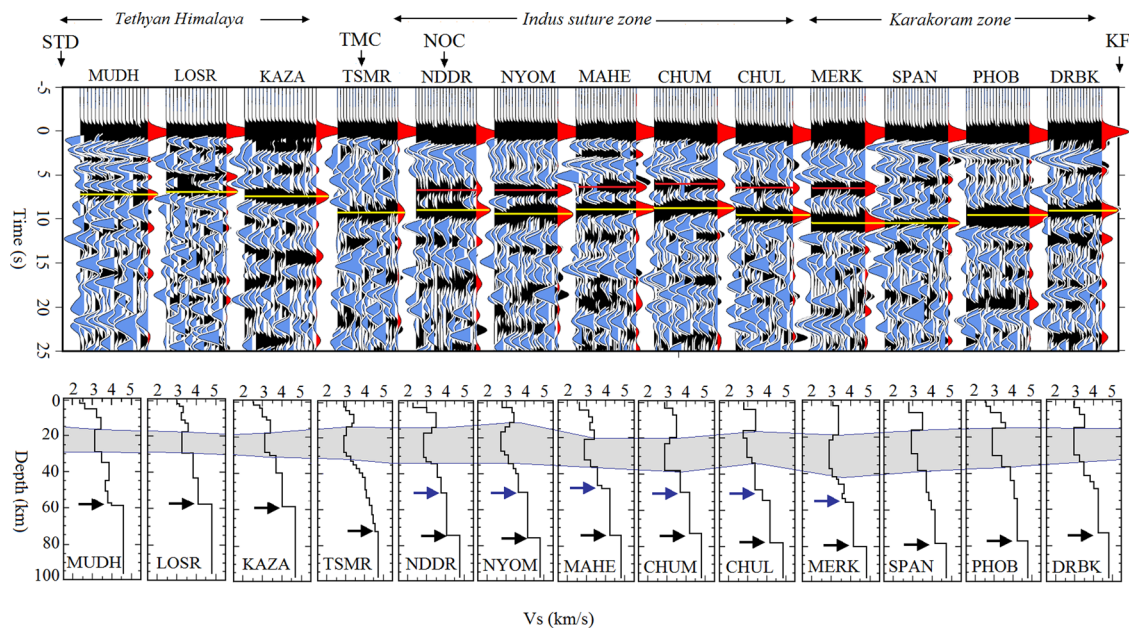


Figure 8. In the upper panel, examples of time section plot of radial RFs with clear record of Moho converted P_s phase at each station is shown. The Moho interface is marked by yellow lines. The strong intracrustal converted phases observed at six stations are marked by red lines. The stack receiver function at each station is shown by red colour. The major tectonic features: South Tibetan Detachment (STD), Tethyan Himalaya, Indus Suture Zone, Tso-Morari Crystalline Complex (TMC), Nidar Ophiolitic Complex (NOC), Karakoram Fault (KF) are marked in the figure. The inverted velocity models corresponding to each station is shown in the lower panel with arrow marks showing Moho (black arrow) and the mid-crustal converting layer observed at six stations (blue arrow). The intracrustal low-velocity layer (IC-LVZ) is marked by the grey shaded area.

Table 1. Locations of seismological stations used for $H-K$ stacking analysis along with corresponding values of estimated thickness of upper crust (i.e. surface to mid-crustal layer, H_1) and entire crustal (i.e. surface to Moho discontinuity, H_2) and corresponding Poisson's ratios (σ_1 and σ_2) at each station.

| Station name | Station code | Latitude ($^{\circ}$ N) | Longitude ($^{\circ}$ E) | Elevation (m) | Thickness from surface to mid-crustal layer (H_1) in km | Poisson's ratio (σ_1) | Thickness of entire crust (H_2) in km | Poisson's ratio (σ_2) |
|--------------|--------------|--------------------------|---------------------------|---------------|---|--------------------------------|---|--------------------------------|
| Nidar | NDDR | 33.142 | 78.599 | 4235 | 47.0 | 0.317 | 75 | 0.284 |
| Nyoma | NYOM | 33.222 | 78.654 | 4185 | 47.3 | 0.315 | 76 | 0.293 |
| Mahe | MAHE | 33.261 | 78.499 | 4170 | 45.9 | 0.316 | 75 | 0.280 |
| Chumathang | CHUM | 33.362 | 78.338 | 4013 | 47.8 | 0.303 | 73 | 0.294 |
| Chushul | CHUL | 33.596 | 78.647 | 4342 | 48.4 | 0.297 | 78 | 0.290 |
| Merak | MERK | 33.804 | 78.591 | 4232 | 48.2 | 0.296 | 80 | 0.303 |

this study profile clearly indicates NE dipping nature of the Indian Moho. Beneath the Ladakh batholith Moho is characterized by NW–SE dipping interface.

6.2 Moho beneath ISZ

The strong azimuthal variation of Moho converted P_s phase across ISZ, NOC and TMC reflects tectonic complexity beneath the region where two continental plates are sutured together subsequent to intercontinental collision and underthrusting of the Indian Plate. Efficiency of the P_s conversion at Moho for teleseismic waves reaching different stations is sensitive to the subsurface structure at conversion (piercing) points. Inversion carried out for RFs of those earthquakes piercing the ISZ shows gradational change in shear wave velocity at the depth of Moho (example is shown at Fig. 3d). Usually Moho is considered as an interface where a step jump in shear wave velocity takes place from crust to upper mantle. This observation indicates some disruption in the crust–mantle boundary,

possibly due to large scale deformation originated by India–Asia collision at deeper depth beneath the Suture Zone. Intensive crust–mantle interaction might have created the intricacy to observe the unique characteristics of the crust–mantle boundary.

6.3 Estimation of melt percentage

Caldwell *et al.* (2009) have estimated the percentage of partial melt in the mid-crust from the Himalayan fold and thrust belt through the Tethyan Himalaya and the Trans-Himalayan suture zone. Based on the experimentally obtained relationship between shear wave velocities and melt percentage, they have inferred 3–7 per cent and at most 10 per cent partial melt in the Himalayan middle crust. In this study we have adopted a similar approach to that of Caldwell *et al.* (2009), where the ratio between the minimum (V_s^L) and maximum shear wave velocity (V_s^0) has been calculated for different tectonic zones and then has been compared with corresponding melt percentage derived from studies of Takei (2000) and Watanabe (1993).

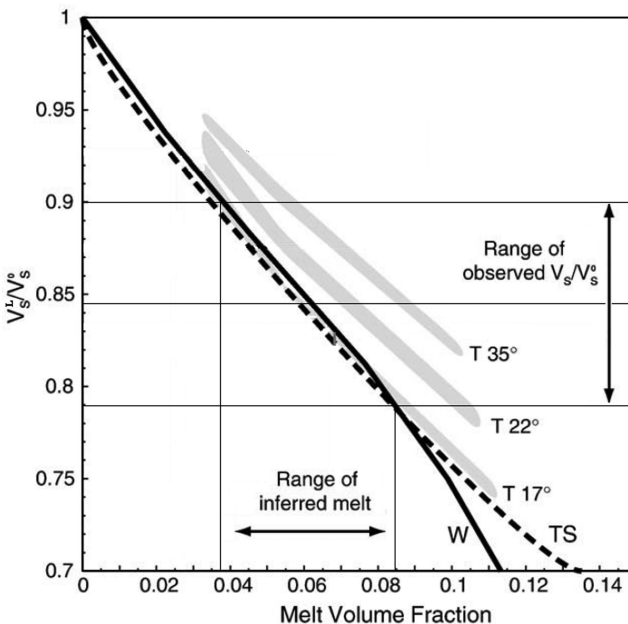


Figure 9. Proportional velocity reduction (V_s^L/V_s^0) vs. melt volume fraction (after Caldwell *et al.* 2009). V_s^L and V_s^0 are calculated as shown in Fig. 3(e). Vertical lines indicate proportional velocity reductions in the low-velocity layer (LVL) for the regions with maximum, minimum and median V_s^L/V_s^0 ratios. W: black line is analytical relationship of Watanabe (1993) for randomly oriented triangular melt tubes. T: grey relationships are the analogue experimental results of Takei (2000) for three different wetting angles, 17, 22 and 35°. TS: dashed line is analytical relationship of Taylor & Singh (2002) for the slow propagation direction in a medium containing perfectly aligned oblate spheroids of aspect ratio 10.

The same comparisons were also made by Caldwell *et al.* (2009). Our study shows (Fig. 9) that the velocity reduction we observed can correspond to ~4–8 per cent of partial melt, which is similar to that inferred by Caldwell *et al.* (2009). Beneath the Tethyan Himalayan stations, the percentage of velocity reduction is about 8.4–11.4 per cent which indicates presence of about 4 per cent melt whereas percentage of velocity reduction is about 12–19 per cent beneath the Ladakh seismological stations indicating presence of 4.5–8 per cent melt. The velocity inversions obtained in this study are more vertically resolved than that of Caldwell *et al.* (2009) and it helps to precisely ascertain the extent of the intracrustal LVZ.

4.4 Origin of IC-LVZ

The IC-LVZ observed in this study shows good spatial correspondence with the low resistivity observed in MT study (Arora *et al.* 2007; Fig. 10). Although the MT study cannot clearly distinguish the causing factor of intracrustal low resistivity layer, the low shear wave velocity observed in this study coupled with unusual high crustal Poisson's ratio beneath the region indicates presence of fluid/partial melt (Hazarika *et al.* 2013). Observed shear wave velocity reduction of about 10–19 per cent in the IC-LVZ with high Poisson's ratio cannot be explained by presence of only solid or dry crustal rocks (Christensen 1996; Caldwell *et al.* 2009). The plausible mechanisms of origin of the IC-LVZ beneath the studied profile are discussed as follows.

4.4.1 The Tethyan Himalaya zone

Our stations located at Kaza, Mudh and Losar, lie within the Tethyan Himalayan zone and RF analysis at these stations shows a distinct IC-LVZ at ~15–25 km depth. Whether the LVZ extends to the south of the suture zone, in to the Tethyan Himalaya has been debated in the past. Caldwell *et al.* (2009) have shown that a mid-crustal LVZ extends from the trans-Himalayan suture zone to the Tethyan Himalaya and the Himalayan thrust belt. On the other hand, Rai *et al.* (2009) have shown that a zone of low attenuation (Q) is confined only to the trans-Himalayan suture zone and does not extend southwards towards the Tethyan Himalaya and the Himalayan thrust belt. Our observation supports the inference of Caldwell *et al.* (2009) and shows presence of mid-crustal low velocity zone in the Tethyan Himalaya as well (Fig. 11a). This low velocity zone is most likely formed due to presence of mid-crustal partial melts/fluids.

4.4.2 Indus suture zone

In this study, the region consisting of the Tso Morari massif, the Zildat Ophiolitic Mélange and the Nidar Ophiolitic Complex is considered as the ISZ. Similar to the Tethyan Himalayan zone to its south and the Ladakh magmatic arc complex to its north, the suture zone also shows presence of a LVZ at mid-crustal depth. The Tso Morari region is also characterized by hot springs in Puga valley and MT investigation carried out in the past suggests a low resistivity layer, which can possibly be correlated with a high temperature zone of partial melts, at 2–6 km depth (Harinarayana *et al.* 2006).

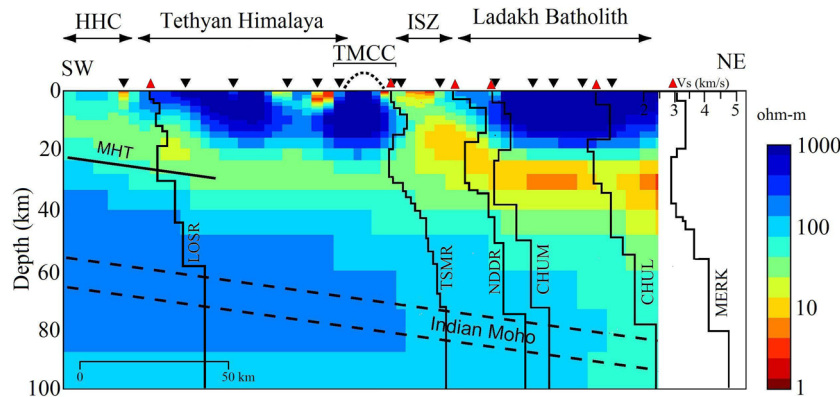


Figure 10. Inverted shear wave velocity models obtained at few seismic stations (shown by red triangle) are projected onto the MT profile of Arora *et al.* (2007). The low-velocity layer (LVL) obtained in this study shows good spatial correspondence with the low-resistivity layer inferred from the MT data. The inverted triangles are the MT stations of Arora *et al.* (2007). The extent of Main Himalayan Thrust (MHT) and the Indian Moho locations are from Arora *et al.* (2007) and Rai *et al.* (2006), respectively. The Higher Himalayan Crystalline zone is marked as HHC.

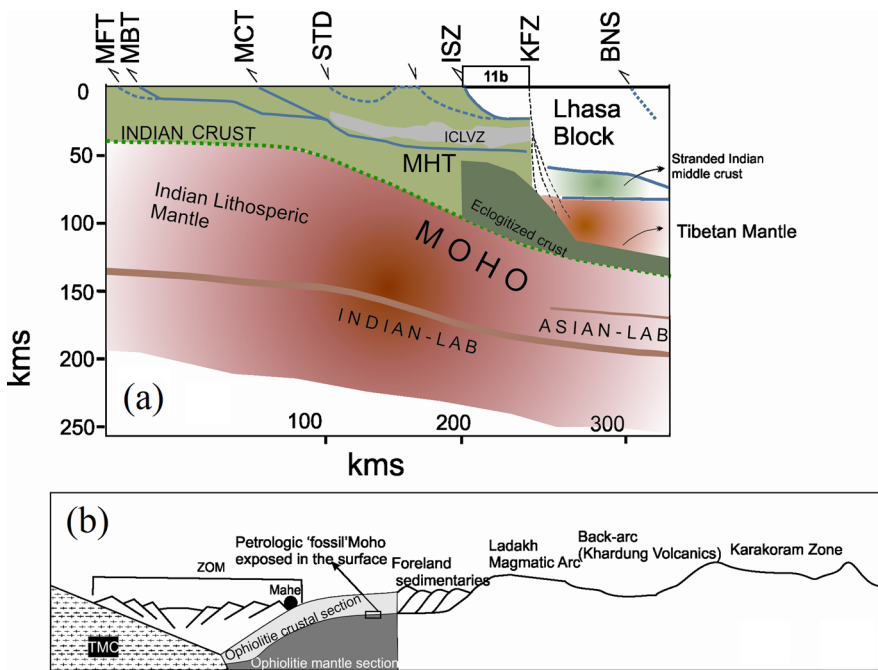


Figure 11. (a) Cartoon showing the subsurface structures of the Indo-Eurasian collisional zone in the trans-Himalaya (modified after Klemperer *et al.* 2013). Depth and extent of the intracrastal low velocity zone (ICLVZ), Moho and eclogitized Indian crust are from this study. The detail subsurface structures, stranded Indian crust and the depth of penetration of the Karakoram fault zone (KFZ) are taken from Klemperer *et al.* (2013). Extent of the Indian Moho beneath Tibet and the LAB (lithosphere–asthenosphere boundary) are taken from Kind & Yuan (2010) and Zhao *et al.* (2011). MFT, main frontal thrust; MBT, main boundary thrust; MCT, main central thrust; STD, south Tibetan detachment; ISZ, Indus suture zone; KFZ, Karakoram fault zone; BNS, Banggong Nujiyang suture. (b) Inset in between ISZ and KFZ shows the surface lithological cross-section of the Suture Zone in detail. TMC, Tso Morari Crystallines; ZOM, Zildat Ophiolitic Mélange.

Following the study of Harinarayana *et al.* (2006) and Azeez & Harinarayana (2007) detected a mid-crustal low resistivity (~ 50 Ohm.m) layer in the suture zone, which they have attributed to the presence of partial melts. The detection of partial melt at mid-crustal depth usually supports the ‘channel flow’ hypothesis that suggests partial melting of the subducting Indian crust and its subsequent return to the foreland surface through mid-crustal channels (Grujic *et al.* 1996; Nelson *et al.* 1996; Beaumont *et al.* 2001). On the other hand, low velocity or low resistivity zones detected in suture zones are sometimes attributed to serpentinite as well. Low velocity zone in this study area could also have formed by partial melts generated due to decompression melting of the Tso-Morari gneiss (De Sigoyer *et al.* 1997; Guillot *et al.* 1997) due to its exhumation that released volatile rich fluids (Fig. 2a; Sen *et al.* 2013). It is worth noting that, unlike the South Tibetan Detachment zone or the Karakoram zone, no Miocene leucogranite plutons are present in the suture zone that can be correlated with mid-crustal partial melts. The leucogranite plutons are considered as an evidence of mid-crustal partial melts and have been correlated with high attenuation and low velocity in the High Himalaya (Ashish *et al.* 2009). The suture zone is lithologically distinct from the rest of the tectonic zones and is dominated by serpentinites and hydrated ultramafic rocks (Fig. 11b). Our observations (Fig. 2) and past geological studies reported widespread serpentinitization in the ISZ and TMC region (Guillot *et al.* 2000, 2001; De Sigoyer *et al.* 2004). The presence of serpentine and other hydrous minerals affect the physical properties of the litho-units, for example decrease of shear wave velocity and increase of Poisson’s ratio (Christensen 1996). The Poisson’s ratio estimations in this study clearly indicate unusual high value (≥ 0.30) in the mid-crust (above ~ 47 – 50 km) which is rare in crustal rocks, except for serpentinite which can be as high as 0.35 (Chevrot & van

der Hilst 2000). Based on high Poisson’s ratio and presence of wide spread serpentinitization in the ZOM and NOC (Fig. 2), presence of serpentinite seems a plausible explanation for the LVZ at the suture zone. However, past studies have shown that serpentinite has low to moderate conductivity (Bedrosian 2007). Even at dehydration temperatures, the conductivity of serpentinite rises only to 0.01 S m^{-1} (Bruhn *et al.* 2004). Serpentinite may show higher conductivity provided it has high porosity or high content of magnetite along its grain boundaries (Stesky & Brace 1973). Presently, we do not have any information regarding the petrophysical/mineralogical properties of the serpentinites of the ISZ, which would suggest high porosity or magnetite-rich grain boundaries. Therefore, the mid-crustal low resistivity zone detected by Azeez & Harinarayana (2007) and the LVZ we detected in this study are more likely to be a result of mid-crustal partial melts. The mid crustal layer observed in the velocity models at ~ 47 – 50 km (Fig. 8) probably indicates contact between the serpentinitized ultramafic rocks of ophiolitic (?) origin and the eclogitized Indian continental crust (Fig. 11). Thermopetrological models suggest a similar depth (45 km) for the onset of eclogitization (Bostock 2013). Eclogitization of the TMC also took place at 20 ± 2 Kbar or ~ 45 km depth (Guillot *et al.* 1997). Wittlinger *et al.* (2009) suggested eclogitic zone having a thickness of ~ 19 km and S-wave velocity of 4.73 km s^{-1} in southern Tibet. Our study suggests a thicker (~ 25 km) eclogitized layer having S-wave velocity of 4.0 – 4.2 km s^{-1} in the ISZ. However, both these studies indicate onset of eclogitization at the suture zone at comparable depths.

6.4.3 Ladakh magmatic arc complex

Low shear wave velocity and high Poisson’s ratio in the mid-crustal part beneath the stations over Ladakh batholith and backarc region

(Fig. 1) can be attributed to presence of fluid/partial melt. Partial melt can arise from shear heating (Rabinowicz & Vigneresse 2004), decompressional melting (Kind *et al.* 2002) or the metamorphic fluids released by temperature controlled dehydration reaction (Hyndman & Shearer 1989; Jones 1992). The origin of crustal fluid/partial melt is usually correlated with high heat generation in the Himalayan arc as a result of the India–Asia collision (Hochstein & Regenauer-Lieb 1998). Previous studies also indicated presence of fluid/partial melt in the mid-crust beneath Ladakh (Arora *et al.* 2007; Caldwell *et al.* 2009; Rai *et al.* 2009). Partial melt has a significant effect on the Poisson's ratio, which increases due to decrease in shear wave (V_s) with an increasing fluid fraction (Watanabe 1993; Christensen 1996).

6.4.4 Karakoram zone

The stations located at the Karakoram Fault Zone (e.g. DRBK and PHOB) also show high Poisson's ratio (Hazarika *et al.* 2013) indicating presence of partial melt/fluid. Recent study by Klemperer *et al.* (2013) shows high He^3/He^4 ratio in hot springs of Karakoram terrane that suggests influence of tectonically active mantle in this region. Hence, the low velocity zone detected in Karakoram region can be caused by partial melts/fluids generated at mantle depth and being up welled along the Karakoram shear zone (Fig. 11a).

The TSMR station shows a prominent converter beneath the Moho at a depth of >100 km (Fig. 6a). It is visible from the NE backazimuths where the Moho is not detected. We are not very sure about its tectonic implications. We can speculate that it is either the eclogitized Indian continental crust beneath the Moho in the north, as a north dipping Main Himalayan Thrust (MHT) would cause increasing proportion of Indian continental crust below the Moho, or alternatively, as suggested by Klemperer *et al.* (2013), as the Indian lower crust continue to underthrust beneath Tibet, the Indian middle crust gets ‘stranded’ in a region beneath the Karakoram Fault Zone and the Banggong Nujiyang Suture. It is possible that the converter at >100 km depth below the Moho can also demarcate the interface between the Tibetan mantle and the Indian lower crust (Klemperer *et al.* 2013; Fig. 11a).

7 CONCLUSION

Based on our seismological and geological study in eastern Ladakh, following conclusions are made:

(1) The inverted velocity model suggests NE dipping nature of Indian Moho beneath the study region from ~ 60 km beneath the Tethyan Himalaya to ~ 80 km towards Ladakh and Karakoram fault zone. The Moho is not clearly detected beneath some part of the ISZ, possibly due to deep deformation and crust-mantle interaction at the suture zone.

(2) A prominent intracrustal low velocity zone (IC-LVZ) exists at a depth of ~ 15 – 40 km extending from the Tethyan Himalaya to the Karakoram Fault zone from the south to the north of the ISZ.

(3) Presence of mid-crustal partial melts is the most plausible cause of this IC-LVZ across the Himalayan Orogen.

(4) The velocity reduction observed suggest presence of 4–8 per cent partial melt at mid-crustal depth.

(5) The eclogitized Indian lower crust, overlain by serpentized ultramafics, is detected at 47–50 km depth.

ACKNOWLEDGEMENTS

The authors are thankful to the Director, Wadia Institute of Himalayan Geology (WIHG), Dehradun, India, for providing necessary support to carry out this work. The Wildlife Protection Department, Jammu and Kashmir is sincerely acknowledged for giving permission to carry out the research work in Ladakh. The logistic support provided by Dr C.P. Dorjey in Leh is sincerely acknowledged. Drs V.C. Thakur, S. S. Thakur, Barun Mukharjee and A.K. Singh are thanked for fruitful discussion on geology of the region. Souvik Das, Koushick Sen and Kavita Tripathi are thanked for their help in geological fieldwork. Prof Simon Klemperer and two anonymous reviewers are thanked for their critical review.

REFERENCES

- Ammon, J.C., Randal, G.E. & Zandt, G., 1990. On the nonuniqueness of receiver function inversions, *J. geophys. Res.*, **95**, 15 303–15 318.
- Arora, B.R., Unsworth, M.J. & Rawat, G., 2007. Deep resistivity structure of the northwest Indian Himalaya and its tectonic implications, *Geophys. Res. Lett.*, **34**, L04307, doi:10.1029/2006GL029165.
- Ashish, Padhi A., Rai, S.S. & Gupta, S., 2009. Seismological evidence for shallow crustal melt beneath the Garhwal High Himalaya, India: implications for the Himalayan channel flow, *Geophys. J. Int.*, **177**, 1111–1120.
- Azeez, K.K. & Harinarayana, T., 2007. Magnetotelluric evidence of potential geothermal resource in Puga, Ladakh, NW Himalaya, *Curr. Sci.*, **93**, 323–329.
- Baumont, C., Jamieson, R.A., Nguyen, M.H. & Lee, B., 2001. Himalayan tectonics explained by extrusion of a low-viscosity crustal channel coupled to focused surface denudation, *Nature*, **414**(6865), 738–742.
- Bedrosian, P.A., 2007. MT+, integrating magnetotellurics to determine Earth structure, physical state and processes, *Surv. Geophys.*, **28**, 121–167.
- Bostock, M.G., 2013. The Moho in subduction zones, *Tectonophysics*, **609**, 547–557.
- Bruhn, D., Siegfried, R. & Schilling, F., 2004. Electrical resistivity of dehydrating serpentinite, in Proceedings of the Tectonophysics Session of the American Geophysical Union, San Francisco, 13–17 December 2004.
- Caldwell, W.B., Klemperer, S.L., Rai, S.S. & Lawrence, J.F., 2009. Partial melt in the upper-middle crust of the northwest Himalaya revealed by Rayleigh wave dispersion, *Tectonophysics*, **477**, 58–65.
- Chamoli, A., Pandey, A., Dimri, V.P. & Banerjee, P., 2011. Crustal configuration of the Northwest Himalaya based on modeling of gravity data, *Pure appl. Geophys.*, **168**, 827–844.
- Chevrot, S. & van der Hilst, R.D., 2000. The Poisson ratio of the Australian crust: geological and geophysical implications, *Earth planet. Sci. Lett.*, **183**(1/2), 121–132.
- Christensen, N.I., 1996. Poisson's ratio and crustal seismology, *J. geophys. Res.*, **101**(B2), 3139–3156.
- Coleman, R.G., 1977. *Ophiolites*, Springer-Verlag, 229 pp.
- De Sigoyer, J., Guillot, S., Lardeaux, J.M. & Mascle, G., 1997. Glauconane-bearing eclogites in the Tso Morari dome (eastern Ladakh, NW Himalaya), *Eur. J. Mineral.*, **9**, 1073–1083.
- De Sigoyer, J., Guillot, S. & Dick, P., 2004. Exhumation processes of the high-pressure low-temperature Tso Morari dome in a convergent context (eastern-Ladakh, NW-Himalaya), *Tectonics*, **23**(3), TC3003, doi:10.1029/2002TC001492.
- Gansser, A., 1964. *Geology of the Himalayas*, Wiley Interscience, 289 pp.
- Gokarn, S.G., Gupta, G., Rao, C.K. & Selvaraj, C., 2002. Electrical structure across the Indus Tsangpo suture and Shyok suture zones in NW Himalaya using magnetotelluric studies, *Geophys. Res. Lett.*, **29**(8), 1251, doi:10.1029/2001GL014325.
- Grujic, D., Casey, M., Davidson, C., Hollister, L.S., Kündig, R., Pavlis, T. & Schmid, S., 1996. Ductile extrusion of the Higher Himalayan Crystalline in Bhutan: evidence from quartz microfabrics, *Tectonophysics*, **260**(1–3), 21–43.

- Guillot, S., Hattori, K. & de Sigoyer, J., 2000. Mantle wedge serpentinization and exhumation of eclogites insights from eastern Ladakh, northwest Himalaya, *Geology*, **28**, 199–202.
- Guillot, S., Hattori, K., de Sigoyer, J., Nägler, T. & Auzende, A.L., 2001. Evidence of hydration of the mantle wedge and its role in the exhumation of eclogites, *Earth planet. Sci. Lett.*, **193**, 115–127.
- Guillot, S., Garzanti, E., Baratoux, D., Marquer, D., Mahéo, G. & de Sigoyer, J., 2003. Reconstructing the total shortening history of the NW Himalaya, *Geochem. Geophys. Geosyst.*, **4**(1), doi:10.1029/2002GC000484.
- Guillot, S., de Sigoyer, J., Lardeaux, J.M. & Mascle, G., 1997. Eclogitic metasediments from the Tso Morari area (Ladakh, Himalaya): evidence for continental subduction during India-Asia convergence, *Contrib. Mineral. Petrol.*, **128**, 197–212.
- Harinarayana, T., Azeez, K.K., Murthy, D.N., Veeraswamy, K., Eknath Rao, S.P., Manoj, C. & Naganjaneyulu, K., 2006. Exploration of geothermal structure in Puga geothermal field, Ladakh Himalayas, India by magnetotelluric studies, *J. appl. Geophys.*, **58**(4), 280–295.
- Hazarika, D., Arora, B.R. & Bora, C., 2012. Crustal structure and deformation in the northeast India–Asia collision zone: constraints from receiver function analysis, *Geophys. J. Int.*, **188**, 737–749.
- Hazarika, D., Kumar, N. & Yadav, D.K., 2013. Crustal thickness and Poisson's ratio variations across northwest Himalaya and Eastern Ladakh and its tectonic implications, *Acta Geophys.*, **61**, 905–922.
- Hochstein, M.P. & Regenauer-Lieb, K., 1998. Heat generation associated with collision of two plates: the Himalayan geothermal belt, *J. Volc. Geotherm. Res.*, **83**, 75–92.
- Honegger, K., Dietrich, V., Frank, W., Gansser, A., Thonic, M. & Trommsdorff, V., 1982. Magmatism and metamorphism in the Ladakh Himalayas (the Indus–Tsangpo suture Zone), *Earth planet. Sci. Lett.*, **60**, 253–292.
- Hyndmann, R.D. & Shearer, P.M., 1989. Water in the lower continental crust: modelling magnetotelluric and seismic reflection results, *Geophys. J. Int.*, **98**, 343–365.
- Jones, A.G., 1992. Electrical properties of the lower continental crust, continental lower crust, in *Developments in Geotectonics*, pp. 81–143, eds Fountain, D.M., Arculus, R. & Kay, R.W., Elsevier.
- Kennett, B.L., 1983. *Seismic Wave Propagation in Stratified Media*, Cambridge Univ. Press, 352 pp.
- Kennett, B.L.N. & Engdahl, E.R., 1991. Travel times for global earthquakes location and phase identification, *Geophys. J. Int.*, **105**, 429–465.
- Kind, R. & Yuan, X., 2010. Seismic images of the biggest crash on Earth, *Science*, **329**, 1479–1480.
- Kind, R. et al., 2002. Seismic images of crust and upper mantle beneath Tibet: evidence for Eurasian plate subduction, *Science*, **298**, 1219–1221.
- Klemperer, S.L., Kennedy, B.M., Sastry, S.R., Makovsky, Y., Harinarayana, T. & Leech, M.L., 2013. Mantle fluids in the Karakoram fault: helium isotope evidence, *Earth planet. Sci. Lett.*, **366**, 59–70.
- Kumar, P., Yuan, X., Kind, R. & Kosarev, G., 2006a. The lithosphere–asthenosphere boundary in the Tien Shan-Karakoram region from S receiver functions: evidence for continental subduction, *Geophys. Res. Lett.*, **32**, L07305, doi:10.1029/2004GL022291.
- Kumar, P., Yuan, X., Kind, R. & Ni, J., 2006b. Imaging the colliding Indian and Asian lithospheric plates beneath Tibet, *J. geophys. Res.*, **111**, B06308, doi:10.1029/2005JB003930.
- Langston, C.A., 1979. Structure under Mount Rainier, Washington, inferred from teleseismic body waves, *J. geophys. Res.*, **84**, 4749–4762.
- Leech, M.L., Singh, S., Jain, A.K., Klemperer, S.L. & Manickavasagam, R.M., 2005. The onset of India-Asia continental collision: early, steep subduction required by the timing of UHP metamorphism in the western Himalaya, *Earth planet. Sci. Lett.*, **234**, 83–97.
- Li, Y., Gao, M. & Wu, Q., 2014. Crustal thickness map of the Chinese mainland from teleseismic receiver functions, *Tectonophysics*, **611**, 51–60.
- Ligorria, J.P. & Ammon, C.J., 1999. Iterative deconvolution and receiver-function estimation, *Bull. seism. Soc. Am.*, **89**, 1395–1400.
- Mahéo, G., Bertrand, H., Guillot, S., Villa, I.M., Keller, F. & Capiez, P., 2004. The south Ladakh ophiolites (NW Himalaya, India): an intraoceanic tholeiitic origin with implication for the closure of the Neo-Tethys, *Chem. Geol.*, **203**, 273–303.
- Mukherjee, B.K. & Sachan, H.K., 2004. Discovery of coesite from Indian Himalaya: a record of ultra-high pressure metamorphism in Indian continental crust, *Curr. Sci.*, **81**, 1358–1361.
- Nábělek, J. et al., 2009. Underplating in the Himalaya-Tibet collision zone revealed by Hi-CLIMB experiment, *Science*, **325**, 1371–1374.
- Nelson, K.D. et al., 1996. Partially molten middle crust beneath Southern Tibet: synthesis of Project INDEPTH results, *Science*, **274**(5293), 1684–1688.
- Oreshin, S.I., Kiselev, S.G., Vinnik, L.P., Prakasam, K. S., Rai, S. S., Makeyeva, L. & Savvin, Y., 2008. Crust and mantle beneath western Himalaya, Ladakh and western Tibet from integrated seismic data, *Earth planet. Sci. Lett.*, **271**, 75–87.
- Oreshin, S.I., Vinnik, L.P., Kiselev, S.G., Rai, S.S., Prakasam, K.S. & Treusov, A.V., 2011. Deep seismic structure of the Indian shield, western Himalaya, Ladakh and Tibet, *Earth planet. Sci. Lett.*, **307**, 415–429.
- Owens, T.J., Zandt, G. & Taylor, S.R., 1984. Seismic evidence for an ancient rift beneath the Cumberland Plateau, Tennessee: a detailed analysis of broadband teleseismic P-waveforms, *J. geophys. Res.*, **89**, 7783–7795.
- Rabinowicz, M. & Vigneresse, J.L., 2004. Melt segregation under compaction and shear channelling: application to granitic magma segregation in a continental crust, *J. geophys. Res.*, **B109**, doi:10.1029/2002JB002372.
- Rai, S.S., Priestley, K., Gaur, V.K., Mitra, S., Singh, M.P. & Searle, M.P., 2006. Configuration of the Indian Moho beneath the NW Himalaya and Ladakh, *Geophys. Res. Lett.*, **33**, L15308, doi:10.1029/2006GL026076.
- Rai, S.S., Ashish, A., Padhi, A. & Sarma, P.R., 2009. High crustal seismic attenuation in Ladakh-Karakoram, *Bull. seism. Soc. Am.*, **99**, 407–415.
- Schärer, U., Xu, R.H. & Allegre, C.J., 1984. U-Pb geochronology of Gangdese, Trans Himalaya, plutonism in the Lhasa-Xigaze region, Tibet, *Earth planet. Sci. Lett.*, **69**, 311–320.
- Schulte-Pelkum, V., Monsalve, G., Sheehan, A., Pandey, M.R., Sapkota, S., Bilham, R. & Wu, F., 2005. Imaging the Indian subcontinent beneath the Himalaya, *Nature*, **435**, 1222–1225.
- Searle, M.P. et al., 1987. The closing of Tethys and the tectonics of Himalaya, *Geol. soc. Am. Bull.*, **98**, 678–701.
- Sen, K., Das, S., Mukherjee, B.K. & Sen, K., 2013. Bimodal stable isotope signatures of Zildat Ophiolitic Mélange, Indus Suture Zone, Himalaya: implications for emplacement of an ophiolitic mélange in a convergent setup, *Int. J. Earth Sci.*, **102**, 2033–2042.
- Sen, K. & Collins, A.S., 2013. Dextral transpression and late Eocene magmatism in the trans-Himalayan Ladakh Batholith (North India): implications for tectono-magmatic evolution of the Indo-Eurasian collisional arc, *Int. J. Earth Sci.*, **102**, 1895–1909.
- Srikantia, S.V. & Bhargava, O.N., 1998. *Geology of Himachal Pradesh*, Geol. Soc. India, 406 pp.
- Stesky, R.M. & Breace, W.F., 1973. Electrical conductivity of serpentinized rocks to 6 kilobars, *J. geophys. Res.*, **78**, 7614–7621.
- Takei, Y., 2000. Acoustic properties of partially molten media studied on a simple binary system with a controllable dihedral angle, *J. geophys. Res.*, **105**(B7), 16 665–16 682.
- Tang, C.C., Chen, C.H. & Teng, L.L., 2008. Receiver functions for three-layer media, *Pure appl. Geophys.*, **165**, 1249–1262.
- Taylor, M.A.J. & Singh, S.C., 2002. Composition and microstructure of magma bodies from effective medium theory, *Geophys. J. Int.*, **149**(1), 15–21.
- Thakur, V.C., 1992. *Geology of Western Himalaya*, Pergamon Press, 363 pp.
- Thakur, V.C. & Misra, D.K., 1984. Tectonic framework of the Indus and Shyok suture zones in Eastern Ladakh, Northwest Himalaya, *Tectonophysics*, **101**, 207–220.
- Thakur, V.C. & Virdi, N.S., 1979. Lithostratigraphy, structural framework, deformation and metamorphism of the southeastern region of Ladakh, Kashmir Himalaya, India, *Himalayan Geol.*, **9**, 63–78.
- Vinnik, L.P., 1977. Detection of waves converted from P to SV in the mantle, *Phys. Earth planet. Int.*, **15**, 39–45.

- Watanabe, T., 1993. Effects of water and melt on seismic velocities and their application to characterization of seismic reflectors, *Geophys. Res. Lett.*, **20**(24), 2933–2936.
- Weinberg, R.F. & Dunlap, W.J., 2000. Growth and deformation of the Ladakh batholith, Northwest Himalayas: implications for timing of continental collision and origin of calc-alkaline batholiths, *J. Geol.*, **108**, 303–320.
- Wittlinger, G. *et al.*, 2004. Teleseismic imaging of subducting lithosphere and Moho offsets beneath western Tibet, *Earth planet. Sci. Lett.*, **221**, 117–130.
- Wittlinger, G., Farra, V., Hetényi, G., Vergne, J. & Nábělek, J., 2009. Seismic velocities in Southern Tibet lower crust: a receiver function approach for eclogite detection, *Geophys. J. Int.*, **177**, 1037–1049.
- Zandt, G. & Ammon, C.J., 1995. Continental-crust composition constrained by measurements of crustal Poisson's ratio, *Nature*, **374**, 152–154.
- Zhao, J. *et al.*, 2010. The boundary between the Indian and Asian tectonic plates below Tibet, *Proc. Natl. Acad. Sci.*, **107**, 11 229–11 233.
- Zhao, W. *et al.*, 2011. Tibetan plate overriding the Asian plate in central and northern Tibet, *Nat. Geosci.*, **4**, 870–873.
- Zhu, L. & Kanamori, H., 2000. Moho depth variation in southern California from teleseismic receiver functions, *J. geophys. Res.*, **105**, 2969–2980.

SUPPORTING INFORMATION

Additional Supporting Information may be found in the online version of this article:

Figure S1. Examples of receiver functions plotted as a function of backazimuth recorded at seismological stations (a) MUDH, (b) KAZA, (c) LOSR, (d) NYOM (e) CHUM, (f) CHUL, (g) SPAN and (h) DRBK. The RFs at station located in the Tethyan Himalaya (a–c) show consistent arrival of Moho from all BAZ whereas strong azimuthal variation is observed at stations located in Ladakh region. The Moho Ps phase is marked by red lines.

Figure S2. H – k stack results showing V_p/V_s ratio versus crustal thickness (H) at (a) NDDR, (b) NYOM, (c) CHUM, (d) CHUL and (e) MERK stations. At each station H – k stack result using Ps_1 and Ps_2 are presented in the first as well as in the second column. The Poisson's ratios estimated at station located over ISZ is much higher in middle crust compared to the estimated value for the entire crust. The best estimated H and k values are indicated by the centre of the error ellipse (marked by star) calculated following Zhu & Kanamori (2000). (<http://gji.oxfordjournals.org/lookup/suppl/doi:10.1093/gji/ggu328/-/DC1>).

Please note: Oxford University Press is not responsible for the content or functionality of any supporting materials supplied by the authors. Any queries (other than missing material) should be directed to the corresponding author for the article.